The Effect of Laser Induced Rapid Solidification Structures on the Adhesion and Bonding Characteristics of an Alumina/Silica-Based Oxide With a Vitreous Enamel

J. Lawrence and L. Li.

Manufacturing Division, Department of Mechanical Engineering, University of Manchester Institute of Science and Technology (UMIST), Manchester, M60 1QD, UK.

Correspondence

Dr. Jonathan Lawrence,

Manufacturing Division,

Department of Mechanical Engineering,

University of Manchester Institute of Science and Technology (UMIST),

Manchester,

M60-1QD,

UK.

Tel : (44) 161 236-3311 ext. 2383

Fax : (44) 161 200-3803

e-mail : j.lawrence@stud.umist.ac.uk

ABSTRACT

This present work is concerned with investigating the effects of high power diode laser (HPDL) radiation on the microstructure of an amalgamated alumina/silica-based oxide compound (AOC). The main rapid solidification theories, namely constitutional supercooling and the theory of morphological stability, are used to explain the observed microstructural changes in the AOC resulting from HPDL interaction. Without laser treatment of the AOC surface it proved impossible to fire the enamel onto the AOC. However, wetting experiments using a number of control liquids, by the sessile drop technique, revealed that laser treatment of the AOC surface resulted in the wetting characteristics of the AOC altering sufficiently to allow the enamel to bond to the AOC. Accordingly, HPDL treatment was identified as allowing the vitreous enamel to wet the surface by effecting a decrease in the enamel contact angle from 118^0 to 33^0. Moreover, no discernible difference was seen in the change in contact angle across the range of rapid solidification microstructures obtained. The actual incidence of rapid surface resolidification, and not the degree of rapid surface resolidification, was therefore identified as being the primary influential factor governing contact angle changes. The bonding mechanisms were identified as being principally due to van der Waals forces, however, some evidence of chemical bonding was observed. The work has shown clearly that laser radiation can be used to alter the wetting characteristics of the AOC.

1. Introduction

Although much literature exists for laser rapid solidification processes of metals and alloys [1-3], there is very little with regard to crystalline ceramic materials [4]. The main reason for this being the inherent lack of thermal shock resistance of most ceramic materials coupled with their high melting temperatures and low thermal conductivity [5]. Notwithstanding this, a reasonable understanding of the formation mechanisms of solidified microstructures in ceramic materials such as the AOC, and, the influence of laser processing parameters on the microstructures of such materials during rapid solidification can be gained from considering the basic concepts of solidification. These are principally the theory of Constitutional Supercooling and the theory of Morphological Stability.

An understanding of the interfacial phenomena between vitreous enamels and ceramic materials is of considerable importance, since in many technological applications where vitreous enamels are fired onto ceramic substrates, the performance of the article is directly linked to the nature of the enamel-ceramic interface. Many studies to investigate these phenomena have been carried out, with investigations of the interfacial mechanisms centring mainly around the thermodynamic criterion [6-8], the electronic theory [9] and the occurrence of oxidation [10, 11]. Work examining the phenomena of wettability has been principally concerned with the wettability of zirconia and other oxide ceramics on metals [6-10] as well as the adhesion of silicone sealants to aluminium [12] and the coating of aluminium alloys with ceramic materials [13, 14].

This present work makes use of the main rapid solidification theories to explain the observed microstructural changes in the alumina/silica-based oxide compound (AOC) resulting from high power diode laser (HPDL) interaction, and, the effects thereof on the adhesion and bonding characteristics of the AOC and a vitreous enamel. No attempt is made to determine the relationship between laser parameters and microstructure since such a relationship is known to be extremely complex [15] and beyond the scope and aims of this work. Such work is of great value since the technique has been employed by the authors to enable the sealing of ceramic tile grouts by means of laser enamelling [16].

2. Experimental procedures

2.1 MATERIALS

A newly developed ceramic tile grout compound consisting of mixed vitrifiable oxide powders such as chamotte (mainly SiO_2 (53wt.%) and Al_2O_3 (42wt.%)), Fe_2O_3, MgO, ZrO_2 and ZnO was produced. The oxide powders were sieved to ensure a particle size of less than 75μm, then thoroughly mixed together to ensure homogeneity, along with approximately 50wt% diluted sodium silicate solution so as to form a manageable paste. The AOC was then pasted on to an ordinary Portland cement (OPC) substrate to a thickness of 2mm and allowed to cure at room temperature for 12 hours. The set compound was then irradiated using the HPDL and immediately pasted over with a thin layer (250μm) of commercially available enamel frit (Ferro Ltd.) which, in order to form a manageable paste, was mixed with 20wt.% white spirit. The powder size of the enamel frit was less than 75μm. The enamel frit paste was allowed to cure at room temperature for one to two hours and then irradiated immediately with the HPDL beam.

2.2 LASER PROCESSING PROCEDURE

The laser used in the study was a surgical HPDL (Diomed Ltd.), emitting at 810nm ±20nm and operating in the CW mode with rated optical powers ranging from 0-60 W. The laser beam was delivered to the work area by means of a 4m long, 600μm core diameter optical fibre, the end of which was connected to a 2:1 focusing lens assembly mounted on the z-axis of a 3-axis computerised numerical control (CNC) gantry table. The AOC was irradiated using the defocused high order mode HPDL beam with a beam spot diameter of 1.75mm and laser powers (measured at the workpiece using a Power Wizard power meter) of 20-55 W. Fig. 1 illustrates the laser processing experimental arrangement, where the defocused laser beam was fired across the surfaces of the AOC and the vitreous enamel by traversing the samples beneath the laser beam using the x- and y-axis of the CNC gantry table at speeds ranging from 5-8 mms^{-1}, whilst 3 $lmin^{-1}$ of coaxially blown O_2 assist gas was used to shield the laser optics.

Variations in the HPDL operating parameters (power density and traverse speed) were seen to affect significantly the microstructures obtained within the laser treated areas on the

AOC. The product of power density and interaction time, which can be derived from the beam spot diameter and the traverse speed, yields the specific energy delivered to the AOC surface. As such, it was possible to group the laser generated microstructures into those produced with high (>600 Jcm^{-2}) and medium (500-600 Jcm^{-2}) specific energies; since the microstructures observed within each region were reasonably typical across the group. Obviously laser induced microstructures were generated outside of the selected energy density regions, but, for simplicity these were not considered in the analysis since they do not lie within the optimum process operating parameters [16].

The laser treated specimens were then examined using optical microscopy (Kyowa Ltd), scanning electron microscopy (SEM), energy disperse x-ray analysis (EDX), x-ray photoemission spectroscopy (XPS) and x-ray diffraction (XRD) techniques.

2.3 WETTING AND SURFACE ENERGY ANALYSIS PROCEDURES

To examine the wetting and surface energy characteristics of the AOC two sets of wetting experiments were conducted. The first set of experiments were to simply determine the contact angle between the enamel and the AOC before and after laser treatment. The second set of experiments were control experiments carried out using a variety of liquids with known surface energy properties in order to quantify any surface energy changes in the AOC resulting from laser irradiation.

The enamel-AOC wetting experiments were carried out in atmospheric conditions and relative humidity of approximately 40% with molten droplets of the enamel (600^0C). The temperature of the enamel throughout the experiments was measured using a Cyclops infrared pyrometer. The droplets were released in a controlled manner onto the surface of the AOC (treated and untreated) from the tip of a micropipette, with the resultant volume of the drops being approximately 15 x 10^{-3} cm^3. Profile photographs of the sessile enamel drop were obtained for every 60^0C fall in temperature of the molten enamel drop, with the contact angle subsequently being measured.

The control experiments were carried out using test liquids previously used [12] and with known properties: human blood, human blood plasma, glycerol and 4-octanol. The test

liquids, along with their total surface energy (γ_2) as well as the dispersive (γ_{lv}^{d}) and polar (γ_{lv}^{p}) components, are detailed in Table 1. The experiments were conducted in atmospheric conditions and relative humidity of approximately 40% at a temperature of 20^0C with the temperature of the liquids themselves throughout the experiments also being maintained at 20^0C. The droplets were released in a controlled manner onto the surface of the test substrate materials (treated and untreated) from the tip of a micropipette, with the resultant volume of the drops being approximately 6 x 10^{-3} cm^3. Each experiment lasted for three minutes with profile photographs of the sessile drops being obtained every minute, with the contact angle subsequently being measured.

3. General effects of laser radiation on the amalgamated oxide compound

The AOC in an un-heated state is physically bonded, as opposed to chemically bonded. This, combined with the retention of chemisorbed and physisorbed water (that is water that is bonded into the materials matrix and additional free-water respectively) means that the hardened mass will rehydrate when exposed to water [17, 18]. Heating of the hardened AOC mass fires the waterglass (similar to that of a ceramic material) [17], increasing its strength and enabling it to withstand water exposure. Thus, heating of the AOC is similar in effect to the firing of ceramics, in that the heating causes gradual ceramic 'sintering' of the materials; generally bonding together and stabilising the substances [17, 19]. As such, exposure of the AOC to laser radiation results in rapid heating of the surface, for most materials typically 10^3-10^5 $^0Cs^{-1}$ [20], which will lead to such sintering of the AOC surface with the removal of the pores between the starting particles of the compound, combined with growth together and strong bonding between adjacent particles [21]. Hence a much more consolidated surface is created.

Indeed, from Fig. 2 it can be seen clearly that before laser treatment the surface of the AOC appears coarse, with individual crystals of the constituent components being clearly discernible. After laser treatment (say Fig. 4(a)) there is more surface ordering, with the

surface appearing cellular-dendritic, showing that fusion of the individual particulates has occurred. Such a solidification structure is indicative of rapidly solidified microstructures [22]. Moreover, an XRD analysis of the AOC surface before and after laser treatment revealed that, on the whole, the phases present within the laser treated region were the same, however, their proportions were different. In particular, after laser treatment it was not possible to detect any SiO_2 whilst the Al_2O_3 was depleted. But, an EDX analysis showed that Si and Al were still present in similar proportions on the AOC surface before and after laser treatment. This indicates that partial laser vitrification of the AOC surface has occurred due to the fact that these materials are glass forming elements, and as such, vitrified when irradiated [23-25].

4. Solidification microstructure analysis

4.1 HIGH SPECIFIC ENERGY MICROSTRUCTURES

A typical example of the microstructures obtained in the (a) centre and (b) on the edge of a HPDL treated track on the AOC surface when using a relatively high specific energy are shown in Fig. 3. As one can see from both Fig. 3(a) and Fig. 3(b), the microstructures appear to be indicative of rapid solidification and are dendritic across the entire width of the laser treated track. However, on the edge of track the dendrites appear much finer and elongated. In both instances the structures appear ordered in orientation.

4.2 MEDIUM SPECIFIC ENERGY MICROSTRUCTURES

Fig. 4 shows a typical example of the microstructures obtained in the (a) centre and (b) on the edge of a HPDL treated track on the AOC surface under relatively medium specific energy conditions. Fig. 4(a) shows that a semi-ordered dendritic structure was observed in the centre of the laser track, whilst in contrast, Fig. 4(b) shows a semi-ordered and much finer elongated cell structure being present on the edge of the solidification track. Moreover, both Fig. 4(a) and Fig. 4(b) display a microstructure typical of rapid solidification. In addition, the very light grey area visible in various parts across Fig. 4(b) are believed to be spherulites. Under lower magnification the semi-directional structure observed in Fig. 4(a)

and Fig. 4(b) was seen typically to extend in a perpendicular direction from the edges of the laser melt track, tending inwards towards the centre of the track.

5. Wettability characteristics

5.1 CONTACT ANGLE AND WETTABILITY

As was discussed previously, prior to laser treatment it was not possible to fire the enamel onto the surface of the AOC. This was due to the fact that the contact angle was measured as 118^0, would therefore prevent the enamel from wetting the AOC surface. Indeed, laser interaction with the enamel when placed on the untreated AOC surface simply resulted in the 'balling' of the enamel; the formation of small spheres approximately the diameter of the laser beam itself [26]. One explanation for the fact that laser treatment of the AOC is necessary so that the enamel completely wets and adheres to the surface of the AOC is that the surface resulting from the laser treatment is significantly smoother, with an Ra value of 25.85μm compared with 6.27μm, which will intrinsically effect a reduction in the contact angle [27-29]. Also, wetting will have certainly been influenced by the increase in the O_2 (oxide) content of the AOC surface as a result of the laser treatment, since this is known to increase the likelihood of wetting [10, 11]. Wetting is governed by the first atomic layers of the surface of a material. Thus, in order to determine the exact element content of O_2 at the surface of the AOC, it was necessary to examine the surface using XPS. An increase in the surface O_2 content was experienced by the AOC after interaction with the HPDL regardless of the energy density used, increasing from an initial value of 37.6atomic% to 42.8atomic% after treatment. It is therefore reasonable the assume that the resultant O_2 enrichment of the HPDL treated AOC surface is active in promoting wetting and bonding.

5.2 AMALGAMATED OXIDE COMPOUND SURFACE ENERGY AND ITS DISPERSIVE/POLAR CHARACTER

The intermolecular attraction which is responsible for surface energy, γ, results from a variety of intermolecular forces whose contribution to the total surface energy is additive [30]. The majority of these forces are functions of the particular chemical nature of a certain

material, and as such the total surface energy comprises of γ^p (polar or non-dispersive interaction) and γ^d (dispersive component; since van der Waals forces are present in all systems regardless of their chemical nature). Therefore, the surface energy of any system may be described by [30]

$$\gamma = \gamma^d + \gamma^p \tag{1}$$

And, according to Fowkes [30], the contact angle, θ, for solid-liquid systems can be related to the surface energies of the respective liquid, γ_{lv}, and solid, γ_{sv}, by

$$\cos\theta = \frac{2\left(\gamma_{sv}^{d}\gamma_{lv}^{d}\right)^{1/2} + 2\left(\gamma_{sv}^{p}\gamma_{lv}^{p}\right)^{1/2}}{\gamma_{lv}} - 1 \tag{2}$$

Consequently it is possible to estimate adequately the dispersive component of the AOC surface energy γ_{sv}^{d} by using Equation (2), and plotting the graph of $\cos\theta$ against $(\gamma_{lv}^{d})^{1/2}/\gamma_{lv}$. Thus the value of γ_{sv}^{d} is estimated by the gradient $(=2(\gamma_{sv}^{d})^{1/2})$ of the line which connects the origin ($\cos\theta = -1$) with the intercept point of the straight line ($\cos\theta$ against $(\gamma_{lv}^{d})^{1/2}/\gamma_{lv}$) correlating the data point with the abscissa at $\cos\theta = 1$ [30]. Fig. 5 shows the best-fit plot of $\cos\theta$ against $(\gamma_{lv}^{d})^{1/2}/\gamma_{lv}$ according to Equation (2) for the untreated and laser treated AOC-experimental control liquids system. No difference in the best-fit plots for the high and medium laser energy density treated AOC samples was observed, and so Fig. 5 can be assumed to represent both conditions. Comparing the ordinate intercept points of the untreated and laser treated AOC-liquid systems, it can be seen clearly from Fig. 5 that for the untreated AOC-liquid systems the best-fit straight line intercepts the ordinate closer to the origin. This indicates that, in principle, dispersion forces act mainly at the AOC-liquid interfaces resulting in poor adhesion [30, 31]. In contrast, Fig. 5 shows that the best-fit straight line for the laser treated AOC-liquid systems intercepts the ordinate considerably higher above the origin. This is indicative of the action of polar forces across the interface, in addition to dispersion forces, hence improved wettability and adhesion is promoted [30, 31].

It is not possible to determine the value of the polar component of the AOC surface energy γ_{sv}^{p} directly from Fig. 5. This is because the intercept of the straight line (cos θ against $(\gamma_{lv}^{d})^{1/2}/\gamma_{lv}$) is at $2\left(\gamma_{sv}^{p}\gamma_{lv}^{p}\right)^{1/2}/\gamma_{lv}$, and thus only refers to individual control liquids and not the control liquid system (i.e. all four control liquids). However, it has been established that the entire amount of the surface energies due to dispersion forces either of the solids or the liquids are active in the wettability performance [30, 32]. Thus by employing a similar technique to that used by Gutowski *et al.*[12] and Agathopoulos *et al.* [33], it is possible to determine γ_{sv}^{p} for the untreated and laser treated AOC.

Table 2 details the values determined for γ_{sv}^{d} and γ_{sv}^{p} for both the untreated and laser treated AOC. Clearly the HPDL treatment of the surface of the AOC leads to a reduction in the total surface energy γ_{sv}, whilst increasing the polar component of the surface energy γ_{sv}^{p}, thus improving the action of wetting and adhesion. Such changes in the surface energy of the AOC after laser treatment are due to the fact that HPDL treatment of the surface of the AOC results in partial vitrification of the surface [23-25] ; a transition that is known to effect a reduction in γ_{sv} and an increase in γ_{sv}^{p} [33].

It is important to note that because of the long range ionic interactions in the AOC and the composite nature of the interfaces between the AOC and the liquids, it is highly likely that the thermodynamically defined total solid surface energy , γ, as defined in Equation (1), will be higher than the sum of the dispersive, γ^{d}, and the polar, γ^{p}, components of the surface energy. Although the increase in (excess) surface free energy will probably be less than the increase in the total lattice energy. On the other hand an absorbed liquid layer may shield the ionic fields substantially. As such, the determined surface energies should be considered as being semi-empirical. Notwithstanding this, as the studies by Gutowski *et al.*[12] and Agathopoulos *et al.* [33] found, it is reasonable to conclude that HPDL treatment of the AOC surface has caused an increase in the polar component, γ^{p}, of the surface energy.

6. Bonding mechanisms

Based on the nature of the attractive forces existing across the liquid-solid interface, wetting can be classified into the two broad categories of physical wetting and chemical wetting. In physical wetting the attractive energy required to wet a surface is provided by the reversible physical forces (van der Waals). In chemical wetting adhesion is achieved as a result of reactions occurring between the mating surfaces, giving rise to chemical bonds [34]. In either case, the driving force for wetting is the reduction of the surface free energy of the solid AOC by the liquid enamel (γ_{sv} - γ_{sl}). Spreading requires the additional contribution to the driving force of the free energy of the interfacial reaction [35].

In practice, complex combinations of various bonding mechanisms actually occur, varying according to the types of materials used [34]. For the AOC and the enamel, the mechanisms involved in ceramic-glass bonding are reasonably applicable. These principally include physical bonding (van der Waals forces), chemical bonding (oxide transformation and oxide bridging) and on a very small scale, electrochemical reactions such as the redox effect due to the presence of ferric oxides within the AOC reacting with other oxides in the enamel [34]. In the particular case of the AOC and the enamel, the bonding mechanism is principally the result of physical forces. This is because adhesion between many materials is assured by electron transfer and is therefore related to bandgap energy [9, 11]. Thus, for non-conducting materials, such as the AOC, with large bandgaps, there will be practically no free charges inside the ceramic crystals, even at elevated temperatures. In this case the electron transfer at the interface will not take place since the electron transfer depends exclusively on the concentration of free charges in the ceramic crystal [9]. As a result, the chemical contribution to the work of adhesion is negligible since W_{ad} can be expressed as the sum of the different contributions of the interfacial interactions between the two phases [8].

$$W_{ad} = W_{non-equil} + W_{chem-equil} + W_{vdw} \tag{3}$$

$W_{non\text{-}equil}$ represents the non-equilibrium contribution to the work of adhesion when a chemical reaction takes place at the interface. $W_{chem\text{-}equil}$ is the cohesive energy between the two contacting phases, which is resulted from the establishment of the chemical equilibrium bonds achieved by the mutual saturation of the free valences of the contacting surfaces. W_{vdw}

is the energy of the van der Waals interaction. Consequently, the work of adhesion W_{ad}, is chiefly only resulted from the van der Waals interaction.

The bonding mechanism between the laser treated AOC and the enamel, however, was found to be not entirely due to physical forces. An EDX analysis conducted at the interface between the AOC and the enamel revealed the presence of a small diffusion region which contained elements unique to the AOC (Mg, Zr, etc.) and the enamel (Mn, Ni, etc.). This is perhaps to be expected since enamel glazes on ceramic materials, such as the AOC, are typically bonded as a result of some of the base material dissolving into the glaze [34], with wetting characteristics often being achieved or enhanced by a reaction at the interface at an elevated temperature [35]. Also, when the samples were pulled apart in this region, debris from both components was found on each of the two pieces, indicating the possible action of some form of chemical bonding. However, such evidence could also be seen as indicating that the van der Waals bond between the enamel and the AOC was stronger than the actual cohesive forces within the AOC.

As one can see from Fig. 6, there is no dendritic growth in the bond region which is characteristic of enamels fired onto substrates containing Fe, Si and in particular Co [35]. However, it can be seen that enamel is held firm in the surface irregularities, thus ensuring sound adhesion. Again, such mechanical bonding is typical of enamel glazes on materials [36].

7. Discussion

From Fig. 3 and Fig. 4 it can be seen that the solidification microstructures obtained differ not only with changes in specific energy, but even across the same track. Such differences in microstructure within the same track result from the fact that at the edge of the melt track the solidification rate, R, is low while the thermal gradient, G, is at its steepest, therefore G/R is high along the fusion line of the melt pool. Towards the centre of the melt zone the solidification rate is increased while the thermal gradient is reduced. Consequently G/R rapidly falls off as solidification proceeds towards the centre of the melt zone. This is the result of the high G/R ratio at the interface is just slightly less than that required for stability, that is the degree of constitutional supercooling is smaller, thus different microstructures at

the edges of the solidification melt tracks can be formed. At the centre, however the G/R ratio is comparatively smaller, which, in the instances where high and medium specific energies were used, allows dendritic structures to be formed within the AOC.

But, as Fig. 3 shows, a dendritic structure was observed in the high specific energy solidification track both in the centre (a) and at the edge (b), although the dendrites at the edge appeared much finer and elongated. It is proposed that under the conditions of high specific energy, the G/R ratio in both regions was small enough to ensure that a dendritic microstructure prevailed. In contrast, as Fig. 4 shows, with medium specific energy a dendritic structure was formed only in the centre (a) of the solidification track, whilst on the edge (b) a finer elongated cell structure was observed. From this it would appear that the initial G/R ratio at the edge is high and rapidly diminishes towards the centre, thus, the much finer and elongated oriented structure is formed at the edge, whilst dendrites are produced in the central area. Another possible reason for the formation of the fine elongated structures at the edges of the solidification tracks seen in Fig. 3(b) and Fig.4(b), is the fact that, although the HPDL beam is not truly Gaussian in nature, the power intensity profile of the beam produces a temperature gradient perpendicular to the direction of traverse [20]. As such, the cooling rate, $\dot{T}$ (=$G.R$) of the AOC will be much faster on the edge of the laser track than in the centre, and may therefore give rise to the much finer and elongated microstructures observed on the edges of the laser tracks in Fig. 3(b) and Fig. 4(b).

Indeed, such findings have been reported by a number of workers conducting research into the laser treatment of various ceramics and alloys. Pei *et al.* [37] noted that both equiaxed and dendritic microstructures were obtained in different regions of the same laser clad ZrO_2 layer, concluding that the differences were related to different cooling rates in the various regions of the laser clad ZrO_2 layer. Similar results were obtained by Liu [38] after laser sealing Y_2O_3-ZrO_2 and MgO-ZrO_2 ceramic coatings. Shih *et al.* [39] observed that across a $YBa_2Cu_3O_x$ and laser clad track different microstructures were found in different regions, as did Shieh [40] across a SiO_2-Al_2O_3 laser clad track. Additionally, both workers noted that not only were cellular and dendritic microstructures visible, but also that the microstructures were much finer on the edge of the clad track than in the centre. Such differences in

microstructure type and size were ascribed to the varying degrees of constitutional supercooling, which, according to McCallum *et al.* [41], are inherent in laser processes.

The directionally-solidified nature of the microstructures observed on Fig. 3(b) and Fig. 4(b), which were seen to extend in a perpendicular direction from the edges of the laser melt track, tending inwards towards the centre of the track, is thought to be due, again, to the fact that the HPDL beam intensity is at a maximum in the centre of the profile. Because of this the highest temperatures occur in the centre of the track with the lowest temperatures being experienced on the edge of the laser track. Consequently solidification begins at the edges of the track and develops quickly inwards as the laser beam is traversed away. Such observations of directional-solidification are in accord with those of Easterling [42] during welding process and Bradley *et al.* [43] during CO_2 laser and HPDL treatment of Al_2O_3 based refractory materials.

It is clear that differences in the HPDL operating parameters produce very different microstructures in the AOC. However, despite this there was no discernible difference in the wetting characteristics of the AOC after laser treatment, both with high and medium energy densities. Indeed, as can be seen clearly from Fig. 7, the surface condition of the laser treated AOC has a significant effect on the contact angle. In particular, Fig. 7 indicates that the melting and resolidification (ie. the partial vitrification of the glass forming elements (SiO_2 and Al_2O_3) within the AOC), is an essential prerequisite in order for significant reductions in the contact angle to be realised. As one can see, after the onset of melting at around 475 Jcm^{-2} the contact angle reduces sharply from 113^0 to 33^0, after which no further decrease (or increase) is discernible until the energy density exceeds 725 Jcm^{-2}. After this point a small increase in the contact angle from 33^0 to 39^0 was observed. This increase is probably due to the fact that this energy density level lies outside of the optimum operating conditions used in the experiments, and as such, will cause an increase in the surface roughness which, as was seen earlier, has a small but discernible effect on the contact angle. The mere reordering of the crystals that occurs at power densities below around 450 Jcm^{-2} [44] appears to have only a slight effect on the contact angle, reducing it from 118^0 to 113^0. Nevertheless, such a reduction in the contact angle reveals that laser interaction without the incidence of melting does have a marginal influence on the wettability characteristics of the

AOC. From this finding it would appear that the actual incidence of melting and rapid surface resolidification, and not the degree of rapid surface resolidification, is the primary factor governing contact angle changes.

8. Conclusions

Both the theories of constitutional supercooling and morphological stability were used to explain the observed microstructural changes in the AOC as a result of HPDL interaction. At relatively high energy densities (>600 Jcm^{-2}), the microstructures were found to be solidified, being dendritic and ordered in orientation across the entire width of the laser treated track, with the dendrites on the edge of track appearing much finer and elongated. At relatively medium energy densities (500-600 Jcm^{-2}), the microstructure was seen to be solidified, displaying a semi-ordered dendritic structure in the centre of the laser treated track, whilst on the edge of the solidification track, a semi-ordered elongated cell structure was in evidence. The semi-directional structures were typically observed to extend in a perpendicular direction from the edges of the laser melt track, tending inwards towards the centre of the track. The observed differences in microstructure within the same track can be attributed to the fact that at the edge of the melt pool the solidification rate, R, is low while the thermal gradient, G, is at its steepest, therefore G/R is high along the edge of the laser melt track. Towards the centre of the melt zone the solidification rate is increased while the thermal gradient is reduced. Consequently G/R rapidly falls off as solidification proceeds towards the centre of the melt zone.

Contact angle measurements revealed that because of the wettability characteristics of the AOC, laser surface treatment was necessary in order to allow the enamel to wet and adhere to the AOC surface. As such, the laser treatment of the AOC surface resulted in the contact angle decreasing from 118^0 to 33^0. Wetting, and subsequent bonding, of the enamel to the AOC surface after laser treatment was identified as being due to:

1. The laser sintering/melting of the AOC surface reducing the surface roughness from an Ra value of 25.85μm before laser treatment, to 6.27μm after laser treatment, thus directly reducing the contact angle, θ.
2. The semi-empirically determined increase in the polar component of the surface energy γ_{sv}^{p}, (2.0 mJm^{-2} to 16.2 mJm^{-2}) after laser treatment as a result of the partial laser vitrification of the glass forming elements within the AOC composition, thus improving the action of wetting and adhesion.
3. The increase in the surface (oxide) O_2 content of the AOC resulting from laser treatment was identified as further promoting the action of wetting.

What is more, no discernible difference was seen in the change in contact angle across the range of rapid solidification microstructures obtained. Hence the actual incidence of rapid surface resolidification, and not the degree of rapid surface resolidification, was therefore identified as being the primary influential factor governing contact angle changes

The bonding mechanisms of the enamel to the AOC were identified as being principally the result of van der Waals forces due to the chemical nature of the AOC. However, evidence of some chemical bonding due to some of the base AOC material dissolving into the enamel glaze was observed.

This work demonstrates that it is possible to alter the wetting characteristics of the AOC using the HPDL to facilitate the firing of a vitreous enamel onto the AOC surface, a task not possible without laser treatment. But, moreover, the findings of this work show that with the use of laser radiation it is a distinct possibility that the wetting characteristics of many other materials could be altered.

References

1. R. MEHRABIAN, B.H. KEAR and M. COHEN: in 'Rapid solidification processing, principles and technologies II: Supercooling and rapid solidification microstructures in metals and alloys', (eds. R. Mehrabian, B.H. Kear and M. Cohen), 89-126; 1980, Baton Rouge, Claitors Publishing.

2. W. KURZ and D.J. FUSHER: ‘Fundamentals of solidification’; 1986, Aedermansdorf, Trans Tech Publications.
3. M.C. FLEMINGS: ‘Solidification processing’; 1974 New York, McGraw-Hill.
4. S. MORDIKE: *Trans. of the Powder Metallurgy Association of India*, 1990, **17**, 81-93.
5. J.P. POLLINGER and G.L. MESSING: in Proc. of ‘Emergent process methods for high technology ceramics’; Raleigh, USA, November 1982, 156-167; 1982, Ceramic Society of America.
6. P. NIKOPOULOS and D. SOTIROPOULOU: *J. Mater. Sci. Lett.,* 1987, **6**, 1429-1430.
7. P.R. CHIDAMBARAM, G.R. EDWARDS and D.L. OLSON: *Mater. Trans. B*, 1992, **23**, 215-222.
8. J.G. LI: *Mater. Lett.*, 1995, **22**, 169-174.
9. J.G. LI: *J. Mater. Sci. Lett.*, 1992, **11**, 903-905.
10. M. UEKI, M. NAKA and I. OKAMOTO: *J. Mater. Sci. Lett.*, 1986, **5**, 1261-1262.
11. J.G. LI: *Rare Met.*, 1993, **2**, 84-96.
12. V.W. GUTOWSKI, L. RUSSELL and A. CERRA: in ‘Science and technology of building seals, sealants, glazing and waterproofing: Adhesion of silicone sealants to organic-coated aluminium’, (ed. J.M. Klosowski), 144-159; 1992, Philadelphia, ASTM.
13. X.B. ZHOU and J.T.M. DEHOSSON: *J. de Phys. IV* , 1993, **3**, 1007-1011.
14. X.B. ZHOU and J.T.M. DEHOSSON: *Acta Metall. Mater.*, 1994, **42**, 1155-1162.
15. Z. LIU: Private communication, 1998.
16. J. LAWRENCE, L. LI and J.T. SPENCER: in Proc. of ‘ICALEO’96- Laser materials processing’; Detroit, USA, October 1996, 138-148; 1996, Laser Institute of America.
17. E.P. DEGARMO, J.T. BLACK and R.A. KOHSER: in ‘Materials and processes in manufacturing’, (eds. E.P. DeGarmo, J.T. Black and R.A. Kohser), 379; 1997, Upper Saddle River, Prentice Hall.
18. L. PENNISI: in ‘Engineered materials handbook- Ceramics and glasses’, (ed. S.J. Schneider), 255-259; 1991, Metals Park, ASM International.
19. L.S. O’BANNON: ‘Dictionary of ceramic science and engineering’, 232; 1984, New York, Plenum Press.

20. W.M. STEEN: ‘Laser materials processing’, 147; 1991, London, Springer-Verlag.

21. D.W. RICHERSON: ‘Modern ceramic engineering’, 217; 1992, New York, Dekker.

22. T.Z. KATTAMIS: in ‘Laser in metallurgy’, (eds. K. Mukherjee and J. Mazumder), 1; 1981, New York, AMIE.

23. J. LAWRENCE, L. LI and J.T. SPENCER: *Mater. Sci. & Eng. A*, 1999, **266**, 1067-1074.

24. J. LAWRENCE and L. LI: *J. Phys. D*, 1999, **32**, 1075-1082.

25. J. LAWRENCE and L. LI: *J. Phys. D*, 1999, **32**, 2311-2318.

26. D.L. BOURELL, H.L. MARCUS, J.W. BARLOW and J.J. BEAMAN: *Int. J. Powder Metall.*, 1992, **28**, 369-381.

27. A.B.D. CASSIE and S. BAXTER: *Trans. Faraday Soc.*, 1944, **40**, 546-552.

28. X.B. Zhou and J.Th.M. De Hosson: *J. Mat. Research*, 1995, **10**, 1984-1992.

29. A.W. NEUMANN: *Adv. Colloid Interface Sci.*, 1974, **4**, 438.

30. F.M. FOWKES: *Ind. Eng. Chem.*, 1964, **56**, 40-52.

31. D.K. CHATTORAJ and K.S. BIRDI: ‘Adsorption and the Gibbs surface excess’, 95; 1984, New York, Plenum Press.

32. R.J. GOOD and L.A. GIRIFALCO: *J. Phys. Chem.*, 1960, **64**, 561-565.

33. S. AGATHOPOULOS and P. NIKOLOPOULOS: *J. of Biomed. Mater. Res.*, 1995, **29**, 421-429.

34. V.A. GREENHUT: in ‘Engineered materials handbook- Adhesives and sealants’, (ed. H.F. Brinson), 298-311; 1991, Metals Park, ASM International.

35. J.A. PASK and A.P. TOMISA: in ‘Engineered materials handbook- Ceramics and glasses’, (ed. S.J. Schneider), 482-492; 1991, Metals Park, ASM International.

36. V.V. VARGIN: ‘Technology of enamels’, 49-56; 1965, London, MacLaren & Sons.

37. Y.T. PEI, J.H. OUYANG and T.C. LEI: *Surface & Coatings Tech.*, 1996, **81**, 131-135.

38. Z. LUI: PhD Thesis, Liverpool University, 1991.

39. C.H.S. SHIH, P.A. MOLIAN, R.W. M^{C}CALLUM and U. BALACHANDRAN: *J. of Mater. Sci.*, 1994, **29**, 1629-1635.

40. Y.N. SHIEH, R.D. RAWLINGS and D.R.F. WEST: *J. of Mater. Sci.*, 1994, **29**, 5285-5292.

41. R.W. M^{C}CALLUM, M.J. KRAMER and S.T. WEIR: *IEEE Trans. on Appl. Superconductivity*, 1993, **3**, 1147-1149.

42. K.E. EASTERLING: 'Introduction to the physical metallurgy of welding'; 1992, Oxford, Butterworth-Heinemann.

43. L. BRADLEY, L. LI AND F.H. STOTT: *Appl. Surf. Sci.*, 1998, **138-139**, 522-528.

44. J. LAWRENCE: PhD Thesis, UMIST, 1999.

LIST OF FIGURES

Figure 1

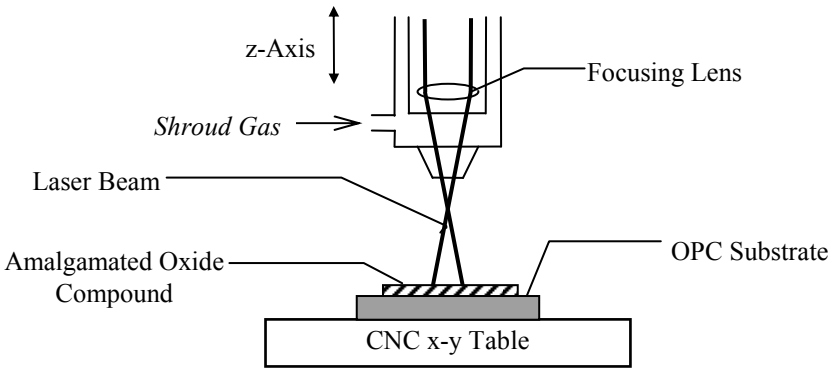
z-Axis
Focusing Lens
Shroud Gas
Laser Beam
Amalgamated Oxide Compound
OPC Substrate
CNC x-y Table

Figure 2

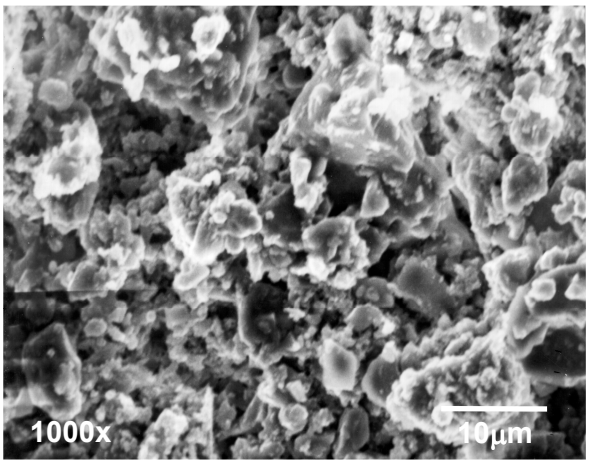

Figure 3

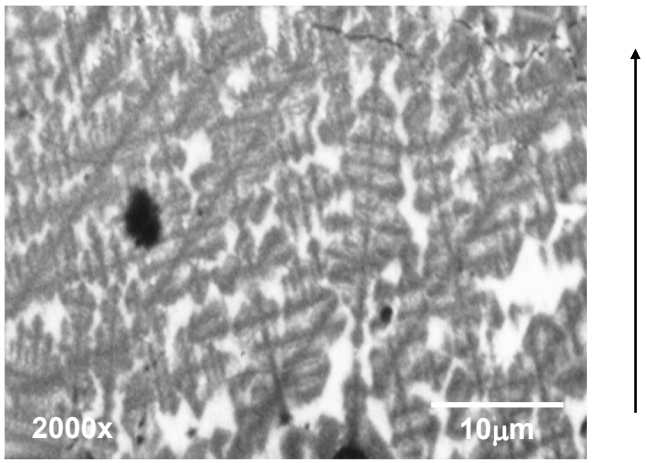

(a)

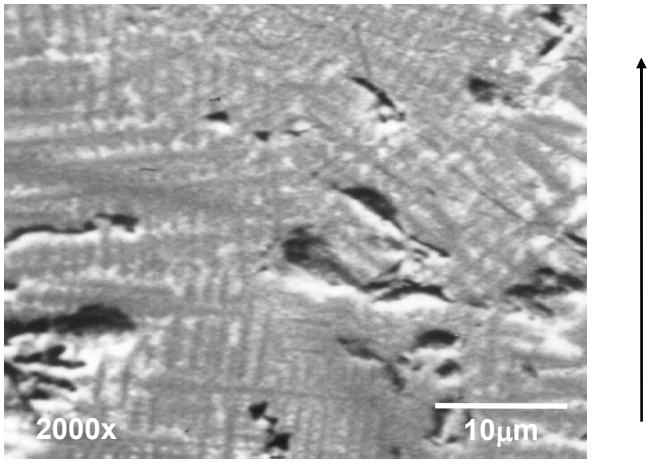

(b)

Figure 4

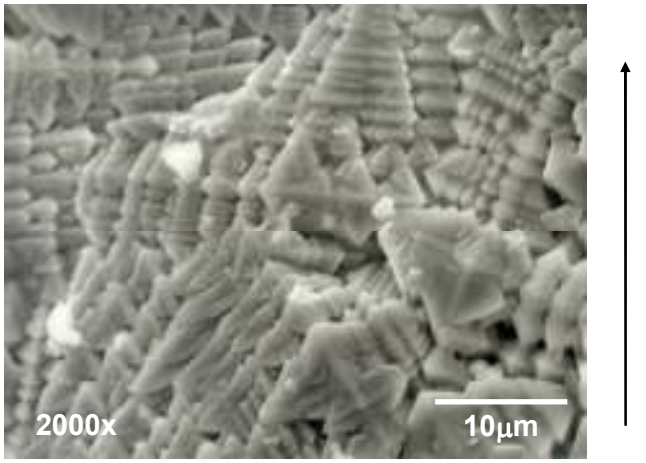

(a)

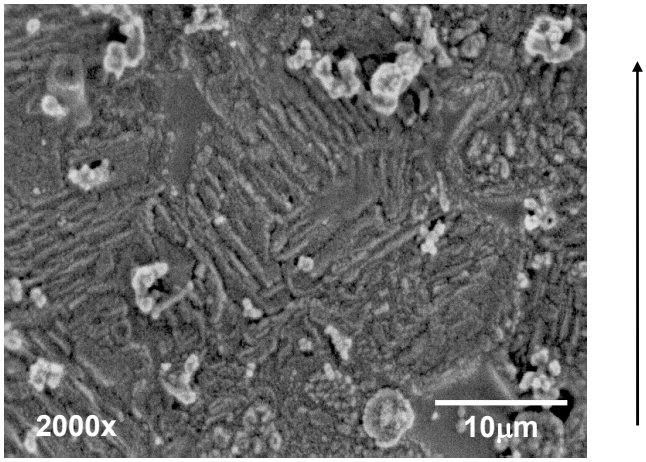

(b)

Figure 5

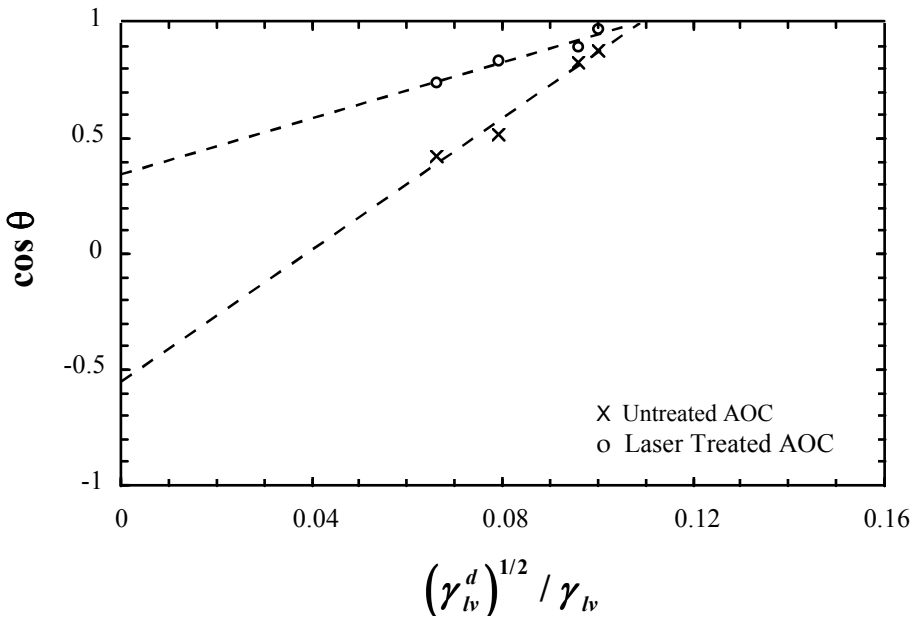
1
0.5
0
-0.5
-1
cos θ
0
0.04
0.08
0.12
0.16
$\left(\gamma_{lv}^{d}\right)^{1/2} / \gamma_{lv}$
X Untreated AOC
o Laser Treated AOC

Figure 6

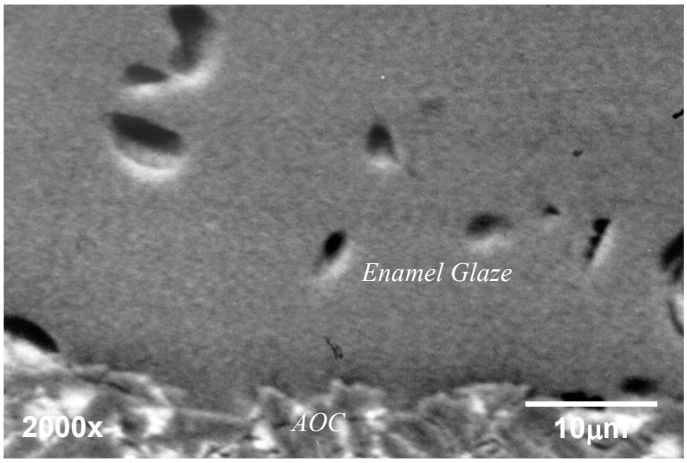

Figure 7

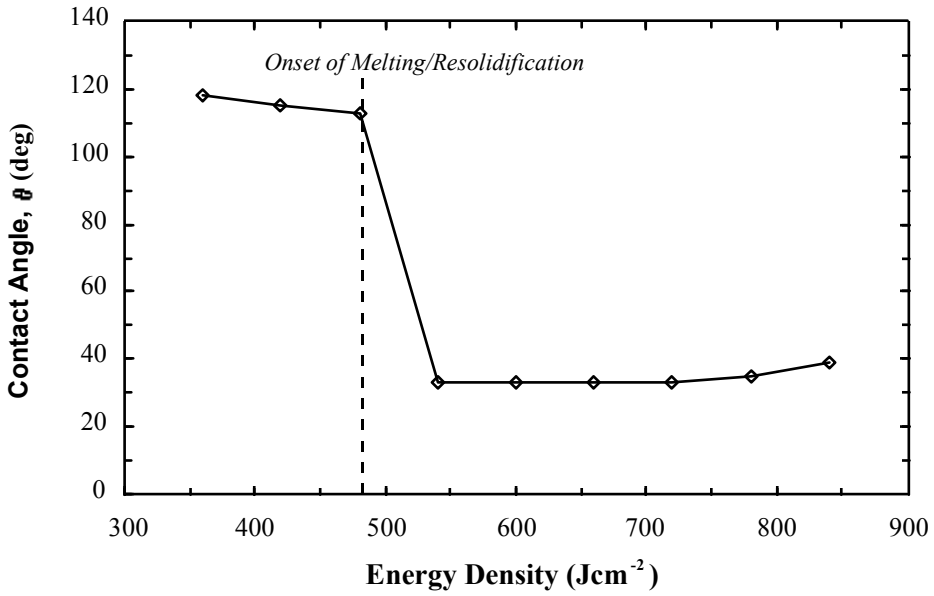
Onset of Melting/Resolidification
Contact Angle, θ (deg)
Energy Density (Jcm-2)
0
20
40
60
80
100
120
140
300
400
500
600
700
800
900

LIST OF TABLES

Table 1

Liquid	γ (mJm^{-2})	γ_{lv}^{d} (mJm^{-2})	γ_{lv}^{p} (mJm^{-2})
Human Blood	47.5	11.2	36.3
Human Blood Plasma	50.5	11.0	39.5
Glycerol	63.4	37.0	26.4
4-Octonol	27.5	7.4	20.1

Table 2

Surface Energy Component	Untreated AOC	HPDL Treated AOC
Dispersive Component, (γ_{sv}^{d})	84.2 mJm^{-2}	89.0 mJm^{-2}
Polar Component, (γ_{sv}^{p})	2.0 mJm^{-2}	25.9 mJm^{-2}